Hindawi Publishing Corporation
Journal of Chemistry
Volume 2016, Article ID 2176576, 11 pages
http://dx.doi.org/10.1155/2016/2176576

Research Article

Liquid-Phase Ethanol Oxidation and Gas-Phase CO Oxidation Reactions over M Doped (M = Ag, Au, Pd, and Ni) and MM′ Codoped CeO_2 Nanoparticles

Yohan Park,[1] Yulri Na,[1] Debabrata Pradhan,[2] and Youngku Sohn[1]

[1]*Department of Chemistry, Yeungnam University, Gyeongsan 38541, Republic of Korea*
[2]*Materials Science Centre, Indian Institute of Technology, Kharagpur 721302, India*

Correspondence should be addressed to Youngku Sohn; youngkusohn@ynu.ac.kr

Received 14 October 2016; Revised 13 November 2016; Accepted 22 November 2016

Academic Editor: Stojan Stavber

Transition metal doped metal oxides have been studied extensively for potential applications to environments and chemical industry. Herein, M doped (M = Ag, Au, Pd, and Ni) and MM′ codoped CeO_2 nanoparticles (NPs) were prepared by a hydrothermal method and their liquid-phase ethanol and gas-phase CO oxidation performances were examined by UV-visible absorption spectroscopy and temperature programmed mass spectrometry, respectively. The ethanol and CO oxidation performances were enhanced greatly by metal-doping and were dependent on the relative concentration of codoped metals. For ethanol oxidation, the concentration of acetaldehyde became saturated at low levels, while that of ethyl acetate continuously increased to become a final major product. For M doped CeO_2 NPs, the ethanol oxidation performance showed an order of Ni < Ag < Pd ≪ Au. For MM′ codoped CeO_2 NPs, the activity of Au doped CeO_2 deteriorated drastically upon adding other metals (Ag, Ni, and Pd) as a cocatalyst.

1. Introduction

The hybridization of metal oxides with transition metals has been performed extensively to increase the catalytic (e.g., CO oxidation) efficiency of the oxides [1–12]. Among the many metal oxides, a reducible CeO_2 support has been studied extensively as a model oxidation catalyst because of its convertible redox states (Ce^{4+}/Ce^{3+}) and oxygen release/storage properties [13–17]. Doped transition metals include Au and Ag [1, 5, 18–32]. Because Au and Ag have the same crystal structure as well as similar lattice constants and metallic bond lengths, they can easily form alloys, which can promote catalytic activity [18, 19, 21]. For CO oxidation over Au/CeO_2 catalysts, Chen et al. reported that the oxidation reactivity of adsorbed CO was independent of the Au particle size, whereas the decomposition reactivity of carbonate, bicarbonate, and formate species was dependent on the particle size; it was higher for larger Au particles [20]. To identify the active sites for Au/CO_2, Nie et al. prepared thiol-protected Au and observed enhanced CO oxidation activity compared to bare Au [1]. Based on this result, they concluded that the active site was the perimeter of Au. Au nanoparticles aggregate easily by sintering at high temperature, which can result in deactivation of Au. To avoid the aggregation of Au, Qi et al. synthesized core-shell $Au@CeO_2$ nanocomposites and observed remarkably enhanced CO oxidation activity [5]. Liu et al. prepared $Ag_xAu_{1-x}@CeO_2$ core@shell nanospheres by galvanic replacement and observed the catalytic CO oxidation activity in the order of $Au@CeO_2$ < $Ag@CeO_2$ ≪ $Ag_{0.41}Au_{0.59}@CeO_2$ < $Ag_{0.64}Au_{0.36}@CeO_2$ [21]. No catalyst shows the best performance in all reaction systems. Fiorenza et al. tested Au/CeO_2, Ag/CeO_2, Cu/CeO_2, $AuAg/CeO_2$, and $AuCu/CeO_2$ catalysts on the oxidation of volatile organic compounds (2-propanol, ethanol, and toluene). They reported that Au/CeO_2 was most active for the oxidation of alcohols, Ag/CeO_2 showed the best efficiency for total toluene oxidation, and $AuAg/CeO_2$ and $AuCu/CeO_2$ showed the highest selectivity to partial oxidation [24]. Studying

alcohol oxidation is very important to understanding of the reaction mechanisms involved in many industrial organic synthetic processes, because of its importance as a fuel [32, 33]. Zhang et al. prepared plum-pudding type Pd@CeO_2 and used it as a visible light photocatalyst for selective oxidation of benzylic alcohols to corresponding aldehydes in a process in which photogenerated electron produced superoxide radicals, thereby facilitating the oxidation [34]. Maldotti et al. emphasized that Au-H species is an important intermediate for alcohol oxidation when Au-CeO_2 catalyst is used [32].

Motivated by these studies, this study examined the catalytic activity of M doped (M = Ag, Au, Pd, and Ni) and MM′ codoped CeO_2 for both liquid ethanol and gas-phase CO oxidation reactions. The catalysts were reacted in a stream of gas-phase CO and liquid-phase ethanol. CO oxidation is the simplest model system understood by a simplified CO + $[O]^* \rightarrow CO_2$ mechanism, while for CH_3CH_2OH oxidation on an oxide support the reactions are very complicated: $CH_3CH_2OH \rightarrow CH_3CH_2O(ad) + H(ad)$, $CH_3CH_2O(ad) + [O]^* \rightarrow CH_3CHO$, $CH_3CHO + [O]^* \rightarrow CH_3COOH$, and ethyl acetate ($CH_3COOCH_2CH_3$) formation via aldehyde and hemiacetal ($CH_3CH(OH)OC_2H_5$). Because the two oxidation reactions have different mechanisms, two systems together were investigated to determine the role of doped metals and the relative concentrations of two different metals.

2. Experimental

Cerium oxide (CeO_2) nanoparticles (NPs) were synthesized by a hydrothermal method, which is described briefly as follows. 10 mL of 0.1 M $Ce(NO_3)_3{\cdot}6H_2O$ (Sigma-Aldrich, 99%) was added to 15 mL of deionized water in a Teflon bottle. Subsequently, 2.0 mL of ammonia (28~30%) solution was added. The solution was fully mixed, and the bottle was tightly capped and placed in an oven (120°C) for 12 hrs. For the synthesis of metal (Ag, Au, Pd, and Ni) doped and codoped CeO_2, stoichiometric amounts (M/M′ = 5/0 mol.%, 1/4 mol.%, 2.5/2.5 mol.%, 4/1 mol.%, and 0/5 mol.% relative to Ce ions) of two different metal solutions were added to the Ce nitrate solution before capping the bottle and placing it into the oven. Upon the reaction for 12 hrs, the final products were cooled naturally and washed repeatedly with deionized water and ethanol several times. The finally collected samples were fully dried in a conventional oven (80°C).

The morphologies of the samples were examined by transmission electron microscopy (TEM, Hitachi H-7600) operated at 100 kV. For this, the samples were mounted onto carbon-coated Cu grids. X-ray diffraction (XRD, PANalytical X'Pert Pro MPD) was performed to examine the crystal structures of the dried powder samples using Cu Kα radiation at 40 kV and 30 mA. The UV-visible (UV-Vis SCINCO Neosys-2000) absorption spectra of the powder samples were recorded. The Fourier transform infrared (FT-IR) spectra were obtained using a Thermo Scientific Nicolet iS10 spectrometer in ZnSe attenuated total reflection mode.

Temperature programmed reduction (TPR) was performed to examine the reducibility of the catalyst powder samples using a Quantachrome CHEMBET equipped with a thermal conductivity detector. The samples were degassed at 150°C for 2 hrs under nitrogen before being tested by TPR. TPR was performed at a heating rate of 20°C/min and a flow rate of 40 mL/min under 5% H_2/N_2 gas stream. CO oxidation tests were performed in a U-tube (inner diameter of 4.0 mm) quartz reactor loaded with 10 mg of the catalyst. The temperature heating rate was set to 10°C/min. The mixed $CO(1.0\%)/O_2/(2.5\%)/N_2$ gas was fed to the reactor at a flow rate of 40 mL/min. The final gas reaction products were monitored using a RGA 200 quadrupole mass spectrometer (Stanford Research Systems, USA).

The liquid-phase ethanol oxidation reaction was performed as follows: 10 mg of the catalyst and 15 mL of ethanol solvent were mixed in a test tube, after which the tube was tightly capped. The test tube was then placed in an oven at 80°C (or 40°C) without stirring. Since we tightly capped the tube, the oxygen supply will be limited at a certain reaction level. After a desired reaction time in the oven, we took the UV-visible absorption spectrum of the solution in the test tube. To detect the final products after the ethanol oxidation, we introduced the solution via a leak valve into the UHV chamber and recorded a mass spectrum.

3. Results and Discussion

The metal (Ag, Au, Pd, and Ni) codoped (M and M′ = 2.5 and 2.5 mol.%, resp.) CeO_2 catalysts were examined by TEM. Figure 1 reveals two different (big and small) size distributions; one was <20 nm and the other was <5 nm. The larger and smaller particles could be attributed to bulk CeO_2 and doped metal nanoparticles, which could be further clearly identified by energy dispersive X-ray spectroscopy and high resolution transmission microscopy. The smaller metal particles could be active sites for the catalytic reactions. The Ag/Au doped sample showed much higher aggregation and the aggregation was found to be in the order of Ag/Au > Au/Ni ~ Au/Pd > Ni/Pd.

Material characterization and CO oxidation were focused only for Ag and Au doped and codoped CeO_2 NPs. Figure 2 presents the powder XRD patterns of undoped CeO_2 and Au and Ag doped and codoped (0/5, 4/1, 2.5/2.5, 1/4, and 5/0 mol.%, resp.) CeO_2 catalysts. For undoped Ce oxide, several major peaks (red filled circles) were observed at 2θ = 28.5°, 33.0°, 47.4°, 56.3°, 59.0°, and 69.3°, which were assigned to the (111), (200), (220), (311), (222), and (400) planes of the cubic (Fm-3m) structure (JCPDS 034-0394) of CeO_2, respectively [11, 12]. The major peak at 2θ = 28.5° showed no critical difference in peak position for all the samples. This means that the crystal lattice of the CeO_2 support was not critically affected by metal-doping. On the other hand, the broadness of the peak was somewhat different, indicating a difference in particle size. The particle sizes of the undoped, 5 mol.% Ag, 4/1 mol.% of Ag/Au, 2.5/2.5 mol.% of Ag/Au, 1/4 mol.% of Ag/Au, and 5 mol.% of Au doped CeO_2 were calculated (using the peak at 2θ = 28.5°) using Scherrer's equation to be 13.0, 14.0, 12.4, 8.0, 10.0, and 8.6 nm, respectively. For the metal doped samples, new peaks (green filled circles) were

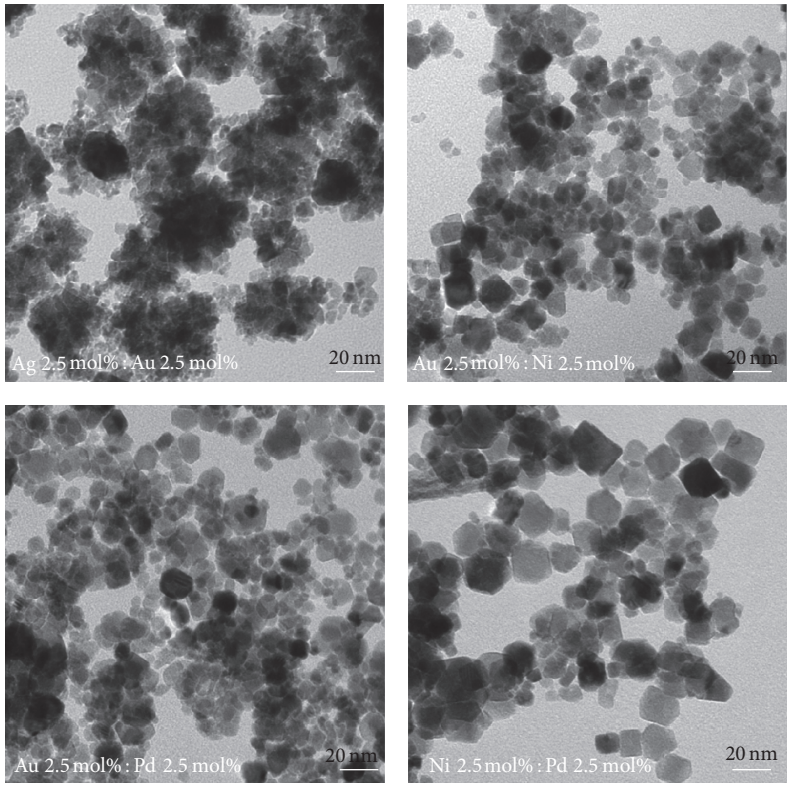

Figure 1: Typical TEM image of Au/Ag, Au/Ni, Au/Pd, and Ni/Pd codoped (2.5 and 2.5 mol.%, resp.) CeO_2 catalysts.

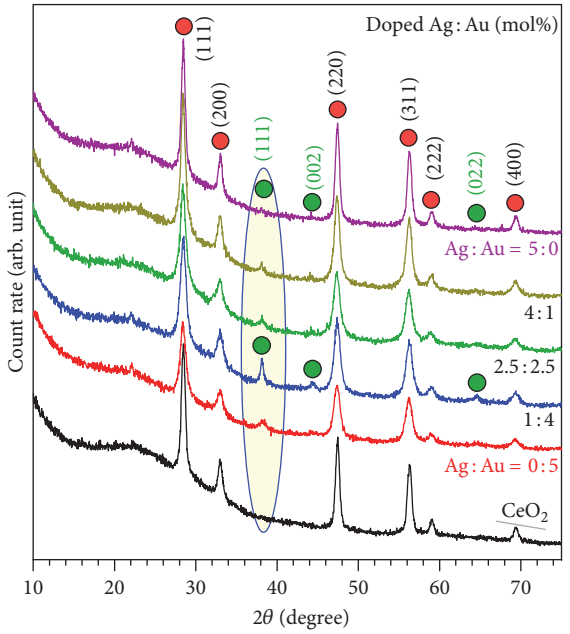

Figure 2: Power X-ray diffraction patterns of undoped CeO_2 and Au and Ag doped and codoped (0/5, 4/1, 2.5/2.5, 1/4, and 5/0 mol.%, resp.) CeO_2 catalysts. The red and green filled circles are of cubic CeO_2 and Au phases, respectively.

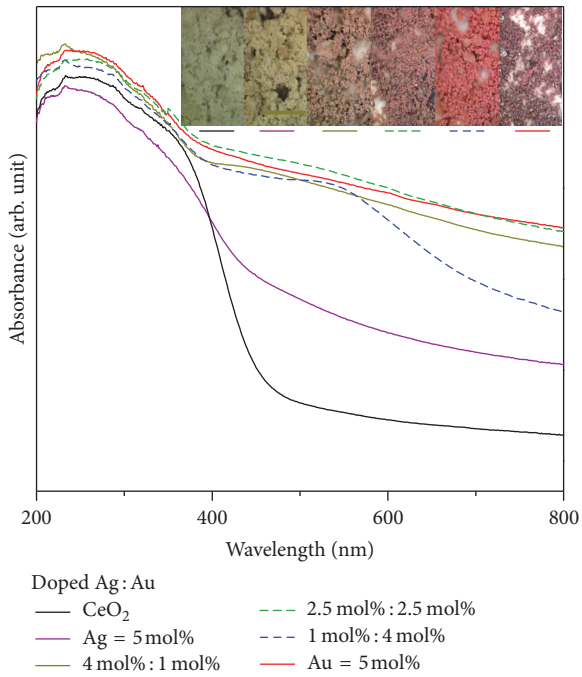

Figure 3: UV-visible diffuse reflectance spectra (expressed in terms of Kubelka–Munk absorbance arbitrary unit) of undoped CeO_2 and Au and Ag doped and codoped (5/0, 0/5, 4/1, 2.5/2.5, and 1/4 mol.%) CeO_2 catalysts. Optical microscopy images (inset) show the colors of the corresponding samples.

observed at 2θ = 38.1°, 44.3°, and 64.6°, corresponding to the (111), (002), and (022) planes of cubic phase metallic Au [5]. The new peaks were the most intense for the Ag/Au (1/4 mol.%) doped sample, which was attributed to the higher crystallinity. No Ag peaks were observed, indicating well-dispersed small amorphous states.

The UV-Vis diffuse reflectance characteristics of the metal doped samples were examined to determine the metal-doping states, as shown in Figure 3. For undoped CeO_2, no significant visible light absorption was observed and the absorption edge was positioned at ~2.9 eV. Upon metal-doping, the absorption in the visible region was increased significantly. For Ag (5 mol.%) doped CeO_2, the color of the powder sample became yellow. The color became reddish as the amount of Au was increased and the UV-Vis absorption in the visible region also increased. For Au (5 mol.%) doped CeO_2, a broad absorption peak was observed at approximately 530 nm, which was attributed to the surface plasmon resonance absorption of Au nanoparticles [30]. For the Ag/Au (4/1, 2.5/2.5, and 1/4 mol.%) doped samples, the absorption in the longer wavelength region was attributed to the formation of larger particles.

Figure 4 presents the FT-IR spectra of undoped CeO_2 and Au and Ag doped and codoped (5/0, 0/5, 4/1, 2.5/2.5, and 1/4 mol.%) CeO_2 nanoparticles. A broad peak was commonly observed at 3400 cm^{-1}, which was attributed to the adsorbed surface OH and/or H_2O species. The maximum of the broad peak was shifted to a shorter wavenumber with increasing the amount of Au. The complicated vibrational peaks observed

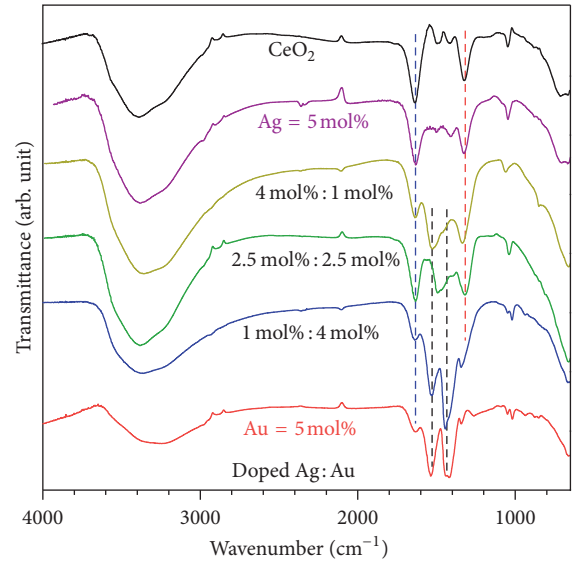

Figure 4: FT-IR spectra of undoped CeO_2 and Au and Ag doped and codoped (5/0, 0/5, 4/1, 2.5/2.5, and 1/4 mol.%) CeO_2.

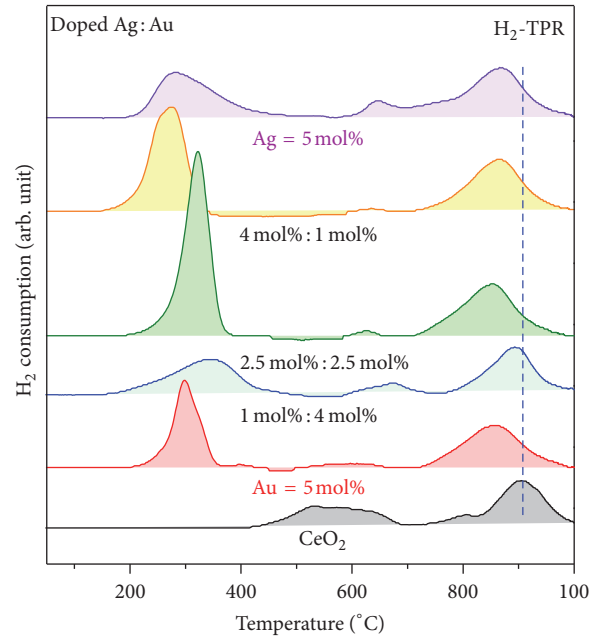

Figure 5: TPR profiles of undoped CeO_2 and Au and Ag doped and codoped (5/0, 0/5, 4/1, 2.5/2.5, and 1/4 mol.%) CeO_2 catalysts.

between 1300 and 1800 cm^{-1} were assigned to C=O, C=C, and COO- functional groups [5], which were dependent on the sample states.

Figure 5 shows the temperature programmed hydrogen reduction (TPR) profiles of the bare and metal doped CeO_2 catalysts. For bare CeO_2, two broad peaks were observed at around 550 and 900°C. The higher temperature peak was attributed to the reduction of bulk oxygen of CeO_2. The lower temperature peak was assigned to the reduction of surface oxygen. The reduction peak for bulk oxygen is

commonly observed for metal doped CeO_2, but at a lower temperature (by ~50°C). In addition, the strong peaks newly appeared below 400°C for the metal doped CeO_2. The peak intensity/position and broadness were dependent on the interactions between the doped metal and the lattice of CeO_2. Because doped Ag and Au are present as the metallic state, the doped metallic nanoparticles could cause the spillover of lattice oxygen by forming Au–O–Ce state to result in easy reduction [19, 24]. Ce^{3+} can be formed from Ce^{4+} by forming Au–O bond and charge transfer from Au to Ce [27]. For Au (5 mol.%) doped CeO_2, the lower TPR peak was observed at approximately 300°C. For Ag/Au (1/4 and 2.5/2.5 mol.%) doped CeO_2, the peak was observed at a somewhat higher temperature with different intensities. For Ag/Au (4/1 and 5/0 mol.%) doped CeO_2, the peak was observed at lower temperatures, indicating stronger interactions with CeO_2.

Figure 6 presents the 1st and 2nd run CO oxidation conversion profiles for undoped CeO_2 and Au and Ag doped and codoped (5/0, 0/5, 4/1, 2.5/2.5, and 1/4 mol.%) CeO_2 catalysts. The CO conversion (%) was calculated using $\{([CO]_{in}-[CO]_{out})/[CO]_{in} \times 100\}$ [35, 36]. $T_{10\%}$ is defined as the temperature corresponding to CO conversion of 10%. As seen in the spectra, the CO oxidation onset position was dramatically different in all samples. For the 1st and 2nd runs of bare CeO_2, $T_{10\%}$ was observed at 405°C. Upon metal-doping, $T_{10\%}$ was lowered dramatically. In the 1st run, $T_{10\%}$ of the 5 mol.% Au and Ag doped samples was observed at 240°C and 352°C, respectively. Compared to that of bare CeO_2, $T_{10\%}$ was lowered by 165°C and 53°C, respectively (bottom left of Figure 6). As the amount of Au was increased, $T_{10\%}$ was observed at a lower temperature. The order of catalytic activity was found to be bare CeO_2 < Ag/Au (5/0 mol.%) < Ag/Au (4/1 mol.%) < Ag/Au (2.5/2.5 mol.%) < Ag/Au (1/4 mol.%) < Ag/Au (0/5 mol.%). In the 2nd run, $T_{10\%}$ was drastically changed for the metal doped samples. $T_{10\%}$ of the 5 mol.% Au and Ag doped samples was observed at 295°C and 262°C, respectively. The Au doped sample showed a 55°C increase in $T_{10\%}$ while Ag doped sample showed a 90°C decrease in $T_{10\%}$. The order of the catalytic activity was bare CeO_2 < Ag/Au (2.5/2.5 mol.%) < Ag/Au (0/5 mol.%) ≈ Ag/Au (4/1 mol.%) < Ag/Au (5/0 mol.%) < Ag/Au (1/4 mol.%). The Ag/Au (1/4 mol.%) showed the highest activity. Compared to $T_{10\%}$ in the 1st run, the Ag/Au (5/0 mol.%) and Ag/Au (1/4 mol.%) samples showed a lower $T_{10\%}$ while other samples showed a higher $T_{10\%}$ in the 2nd run, as shown in the bottom right of Figure 6. In the 2nd run, both the sintering of Au nanoparticles and alloying of two different metals were expected to play a role in determining the activity because the sample had already experienced a high temperature up to 700°C. The colors of the samples were significantly changed after the CO oxidation reactions. Particularly, the colors of the Ag/Au (4/1 mol.%), Ag/Au (2.5/2.5 mol.%), and Ag/Au (0/5 mol.%) became dark grey (or black) after the CO oxidation, unlike other three samples. The corresponding catalysts showed catalyst deactivation in the 2nd run, compared with the 1st run (Figure 6(d)). This indicates that change in oxidation state, carbon residues after reaction, and sintering/alloying of loaded metals are important factors for the determination of catalytic activity. Sasirekha et al. examined CO oxidation under hydrogen-rich conditions for Au and Ag doped and codoped CeO_2 catalysts and reported that the Ag-Ag (5 : 5) doped sample showed the highest CO conversion and selectivity [19]. The enhancement was attributed to bimetallic alloy formation [19, 24]. On the other hand, in the present study, the Ag/Au (2.5/2.5 mol.%) sample showed the poorest activity among the metal doped samples in the 2nd run. This suggests that other factors (e.g., size and relative distributions) are also important for determining the activity. CO oxidation has commonly been understood by $CO(ad) + [O]^* \rightarrow CO_2$ (g), where $[O]^*$ is the active surface oxygen. The surface oxygen is replenished by molecular oxygen present in air. Adsorbed CO is plausibly present at the interface of doped metal and CeO_2, on top of metal, and/or defect sites [31]. The crystalline size (reflecting the surface area) of the samples was estimated using the full width at half maximum of the (111) peak and Scherrer's equation [12]. The order of the size was found to be Ag/Au (2.5/2.5 mol.%), 8.0 nm < Ag/Au (0/5 mol.%), 8.6 nm < Ag/Au (1/4 mol.%), 10.0 nm < Ag/Au (4/1 mol.%), 12.4 nm < bare CeO_2, 13.0 nm < Ag/Au (5/0 mol.%), and 14.0 nm. Based on this, the size was not linearly related with the catalytic activity. For this reason, the metal-loading is important and the metal-support interactions play significant roles in the catalytic activity [37]. In the present study, $T_{50\%}$ for all the samples was observed to be >300°C. Zhang et al. reported significantly lower $T_{50\%}$ for Au/CeO_2 prepared by a deposition-precipitation method [37]. They reported $T_{50\%}$ of 63, 35, and 17°C for untreated, H_2, and H_2-O_2 treated samples, respectively. They concluded that the surface interaction between Au and CeO_2 was the most important factor for the catalytic activity. Li et al. reported $T_{50\%}$ of <150°C for crystalline Cu-CeO_2 (5–8 nm) nanopowders synthesized by a hydrothermal method [38]. The formic acid-treated Co_3O_4-CeO_2 catalysts were reported to show $T_{50\%}$ at 69.5°C for CO oxidation [39]. The CO oxidation catalytic activities for other CeO_2-based catalysts were summarized elsewhere [11].

Ethanol oxidation reaction performances were fully examined for all M doped (M = Ag, Au, Pd, and Ni) and MM′ codoped CeO_2 NPs by UV-visible absorption spectroscopy. Figure 7 shows the UV-Vis absorption spectra of the ethanol solutions reacted at 80°C for 5 days with and without catalysts and with different metal-doping concentration states. Two broad absorption peaks were commonly observed at around 220 and 280 nm, which were tentatively attributed to ethyl acetate ($CH_3COOCH_2CH_3$, EA) and acetaldehyde (CH_3CHO, AcA), respectively, for the oxidation products of ethanol. Further details were discussed below. The EA peak became stronger and increased more sharply than the AcA peak with reaction time. The AcA absorption peak intensity increased slightly, gradually reaching a certain low concentration level. The presence of EA as a major and AcA as a minor product was further confirmed by mass spectrometry (or UV-visible absorption) as discussed in detail below. To examine the temperature effect, we conducted ethanol oxidation experiments at 40°C and 80°C. As expected, the absorbance of the two peaks was dramatically enhanced upon

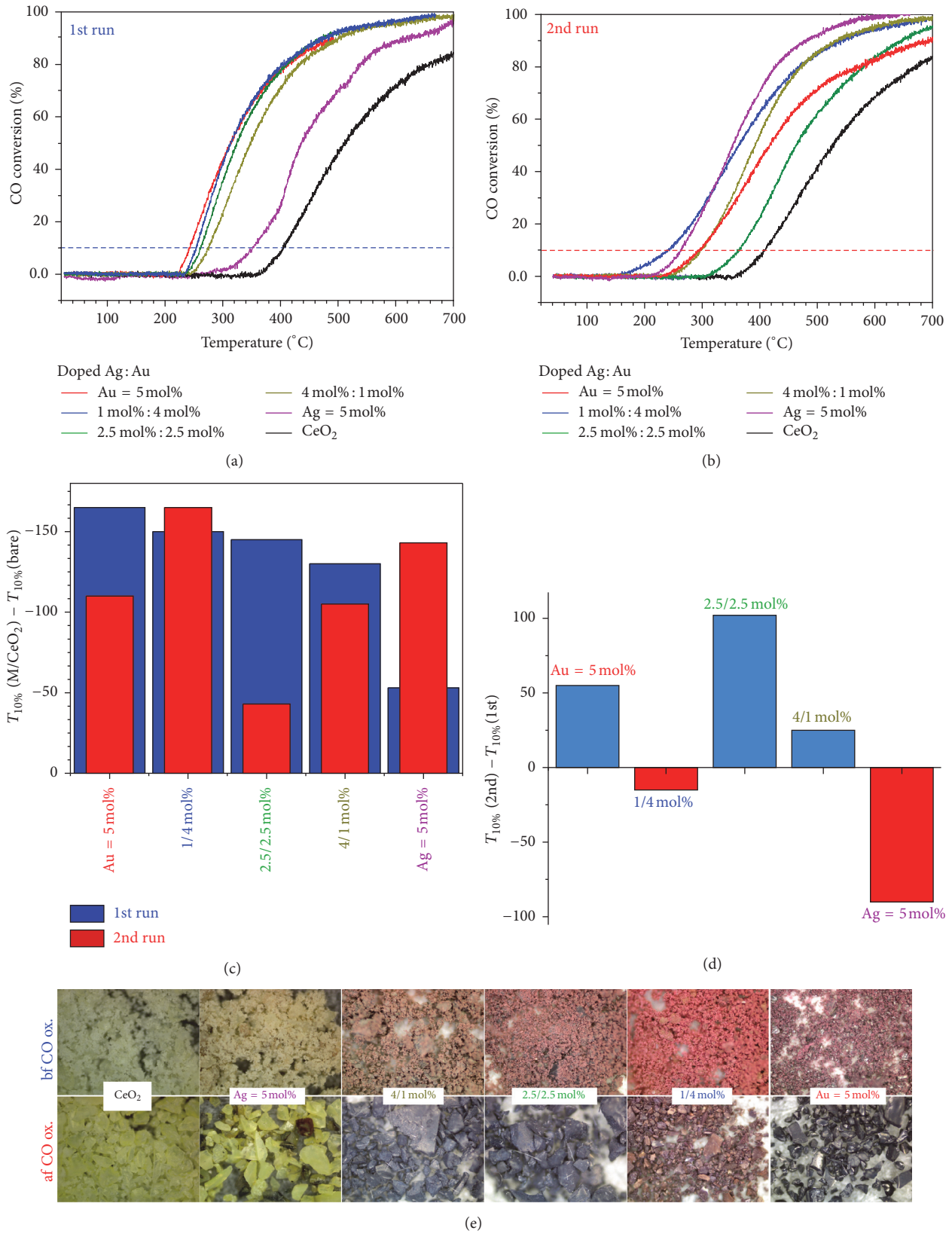

FIGURE 6: 1st (a) and 2nd (b) run temperature programmed CO oxidation conversion (%) profiles (a, b) of undoped CeO_2 and Au and Ag doped and codoped (5/0, 0/5, 4/1, 2.5/2.5, and 1/4 mol.%) CeO_2 catalysts. The difference (c) in $T_{10\%}$ between the metal doped and bare CeO_2 for the 1st and 2nd runs. The difference (d) in $T_{10\%}$ between the 1st and 2nd runs for the metal doped CeO_2 catalysts. Optical microscope images showed the color of the powder samples before and after CO oxidation reactions.

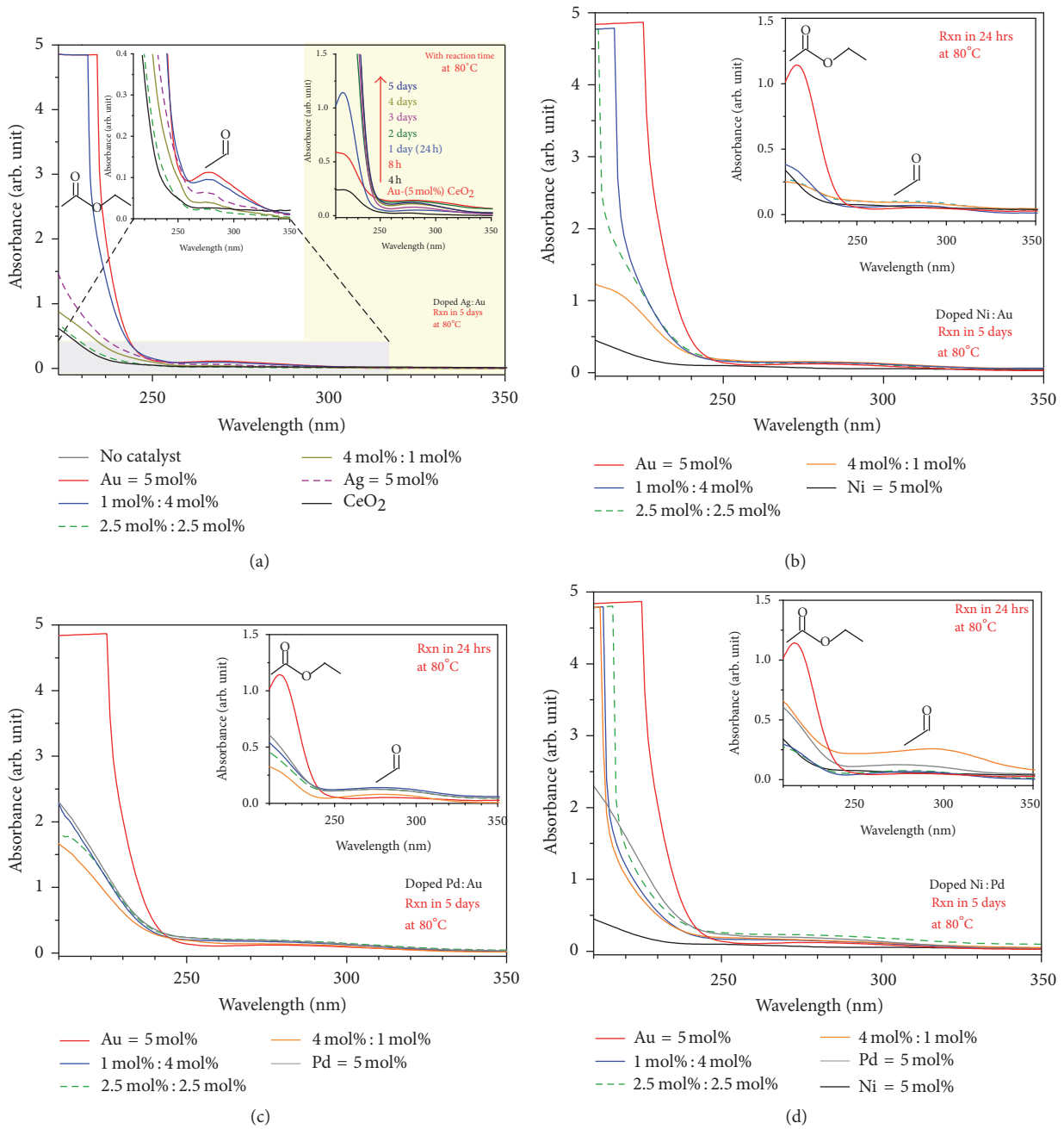

FIGURE 7: UV-visible absorption spectra of the ethanol oxidation with no catalyst, undoped CeO_2, M doped (M = Ag, Au, Pd, and Ni) and MM′ codoped (Ag/Au (a), Ni/Au (b), Pd/Au (c), and Ni/Pd (d)) CeO_2 catalysts at 80°C for 5 days. The left inset in (a) shows the magnified spectra of the grey shadowed region. The right inset in (a) shows the UV-Vis absorption spectra of ethanol oxidation with the 5 mol.% Au doped CeO_2 catalyst at 80°C according to the reaction time.

increasing reaction temperature. Without catalysts, no significant ethanol oxidation occurred, even at high temperature. For further ethanol oxidation experiments, we selected a reaction temperature of 80°C and a total metal-doping level of 5 mol.%.

For Ag and Au doped and codoped samples (Figure 7(a)), a strong absorption peak (below 250 nm) was observed for the Au (5 mol.%) and Au/Ag (1/4 mol.%) doped CeO_2 catalysts. Without a catalyst, no significant absorption peak was observed, even after 5 days. The absorption peak (shown in the right inset of Figure 7(a)) increased with increasing reaction time. This was attributed to an increase in reaction products that contain C=C and/or C=O functional groups. For the other metal doped samples, the absorption peaks were much weaker. In addition to the strong absorption peak, a weaker peak at 280 nm was also observed (in the left inset of Figure 7). The results suggest that at least two reaction products (EA and AcA as mentioned above) were

present in the ethanol solution. The catalytic activity was observed to be in the order of bare CeO_2 ≈ 2.5/2.5 < 4/1 < 5/0 ≪ 1/4 < 0/5 (Ag/Au mol.%). When the concentration of Au was the same as or lower than that of Ag, the activity deteriorated drastically. For Au and Ni doped and codoped samples (Figure 7(b)), the catalytic activity was decreased upon adding Ni as a cocatalyst. The activity was found to be in the order of 5/0 < 4/1 ≪ 2.5/2.5 < 1/4 < 0/5 (Ni/Au mol.%). For Au and Pd doped and codoped samples (Figure 7(c)), the oxidation performance was more greatly decreased upon adding Pd as a cocatalyst and found to be in the order of 4/1 ≤ 2.5/2.5 ≈ 1/4 ≈ 5/0 ≪ 0/5 (Pd/Au mol.%). For Ni and Pd doped and codoped samples (Figure 7(d)), the catalytic activity was observed to be in the order of 5/0 < 0/5 ≪ 4/1 ≈ 1/4 ≤ 2.5/2.5 (Ni/Pd mol.%). The catalytic activity of the Ni/Pd codoped samples showed much higher catalytic activity than those of the single M- (Ni and Pd) doped samples. For comparison of the catalytic activities of single M doped CeO_2 NPs, the ethanol oxidation performance showed an order of undoped ≈ Ni < Ag < Pd ≪ Au. Interestingly, the Ni-doping showed no increase in catalytic activity for ethanol oxidation.

For ethanol oxidation on a metal doped CeO_2 power sample, since the reaction mechanism was much more complicated than expected on a single crystal surface, we propose the following simplified mechanisms, which are discussed in greater detail below [32].

Acetaldehyde, hemiacetal, and ethyl acetate formation from ethanol is as follows:

$$CH_3CH_2O\text{–}H \longrightarrow CH_3CH_2O\,(ad) + H\,(ad) \quad (1)$$

$$CH_3CH_2O\,(ad) + O \text{ species} \longrightarrow CH_3CHO\,(ad) + OH\,(ad) \quad (2)$$

$$CH_3CH_2O\,(ad) - M \longrightarrow CH_3CHO \text{ (minor)} + MH \text{ hydride shift} \quad (3)$$

$$CH_3CHO + O\,(ad) \longrightarrow CH_3COO\,(ad) + H\,(ad) \longrightarrow CH_3COOH \quad (4)$$

$$CH_3COOH\,(ad) + CH_3CH_2OH\,(ad) \longrightarrow CH_3COOCH_2CH_3 + H_2O \quad (5)$$

$$2CH_3CHO\,(ad) \longrightarrow CH_3COOCH_2CH_3 \quad (6)$$

$$CH_3CHO\,(ad) + CH_3CH_2OH\,(ad) \longrightarrow CH_3CH\,(OH)\,OC_2H_5 \text{ (hemiacetal)} \longrightarrow CH_3COOCH_2CH_3 \text{ (major)} + H_2 \quad (7)$$

The rate constant for each step is controlled by the surface area and metal-support interaction (or surface activity). In reaction (1), the O–H bond of ethanol dissociates to form CH_3CH_2O, which may be mainly adsorbed onto the doped metal site. This then turns into adsorbed CH_3CHO via nearby active oxygen species in (2), or the adsorbed CH_3CH_2O on metal desorbs as CH_3CHO (acetaldehyde) in response to a hydride shift reaction in (3) [32, 40]. Although we have no direct evidence of the hydride shift reaction, the reaction process is highly plausible. The acetaldehyde in (4) further precedes oxidation reactions to form CH_3COOH (acetic acid) if active oxygen species are available nearby. Otherwise, the CH_3COOH with ethanol in (5) and $2CH_3CHO$ in (6) react to form $CH_3COOCH_2CH_3$ (ethyl acetate). In reaction (7), CH_3CHO and ethanol form $CH_3CH(OH)OC_2H_5$ (hemiacetal), which is converted to ethyl acetate. Consequently, ethyl acetate ($CH_3COOCH_2CH_3$) is formed as a final oxidation product, which was confirmed by mass spectrometry. In the present UV-Vis spectra, two products of ethyl acetate (major) and acetaldehyde (minor) were observed. For alcohol oxidation on the Au-CeO_2 catalyst, Maldotti et al. reported that the Au-H species is an important intermediate [32]. This indicates that the hydride shift reaction is facilitated by active doped metals. The present study showed that the Au-rich catalyst produced much higher oxidation products and the Au species is more active than other metal species (Ag, Ni, and Pd). The reference UV-Vis spectra (Figure 8(a)) were checked for four plausible ethanol oxidation products; acetaldehyde, ethyl acetate, acetone, and acetic acid and the stronger and weaker peak positions near 220 and 280 nm were assigned to the UV-Vis absorptions of ethyl acetate and acetaldehyde, respectively. Figure 8(b) displays the mass spectrum of the solution sample after reaction relative to those of the reference solvents (ethyl acetate and ethanol). As shown in the mass spectrum, the oxidation product in ethanol matched that of the reference ethyl acetate well. In addition, the smell of the two samples was very similar. As a result, we concluded that the final major product was ethyl acetate. For some other extra mass fragmentation signals (59, 73, and 75 amu), although no reference data were available, the fragmentations appeared to form from the hemiacetal, as shown in reaction (7). Abad et al. extensively studied oxidation of alcohols catalyzed by Au/CeO_2 [40] and proposed a reaction of (7), mentioned above, in which hemiacetal was detected by H-NMR. We have excluded diethyl ether as a major product, even though it could be formed by $2C_2H_5OH \rightarrow C_2H_5OC_2H_5 + H_2O$, because the UV-visible absorption intensity (even measured with 50% solution) was extremely low (Figure 8(a)) when compared with that of the sample. We also detected no fragmentation signals of diethyl ether by mass spectrometry. The acetone formation reaction, $2CH_3CHO \rightarrow CH_3COCH_3$ (acetone) + CO_2 + H_2, was excluded due to absence of the mass signal. Acetic acid as a major product was also excluded because the solution is not acidic, the mass signal is absent, and it did not smell like acetic acid. Table 1 summarizes the sizes of the metal-loaded CeO_2 estimated using Scherrer's equation. As for the CO oxidation, the ethanol oxidation activity was also found to be more loaded metal (and the relative concentrations) dependent than the size-dependent.

4. Conclusion

To increase the catalytic activity of bare CeO_2, the CeO_2 matrix was doped and codoped with Ag, Au, Pd, and Ni by a hydrothermal method. The novelty of the present study

Table 1: Particles sizes of the metal-loaded CeO_2 estimated using Scherrer's equation.

Loaded M/M′	5/0 mol.% (nm)	4/1 mol.% (nm)	2.5/2.5 mol.% (nm)	1/4 mol.% (nm)	0/5 mol.% (nm)
Ag : Au	14.0	12.4	8.0	10.0	8.6
Ni : Au	15.2	12.3	10.6	8.2	8.6
Pd : Au	15.1	12.7	12.1	9.0	8.6
Ni : Pd	15.2	11.1	14.7	12.1	15.1

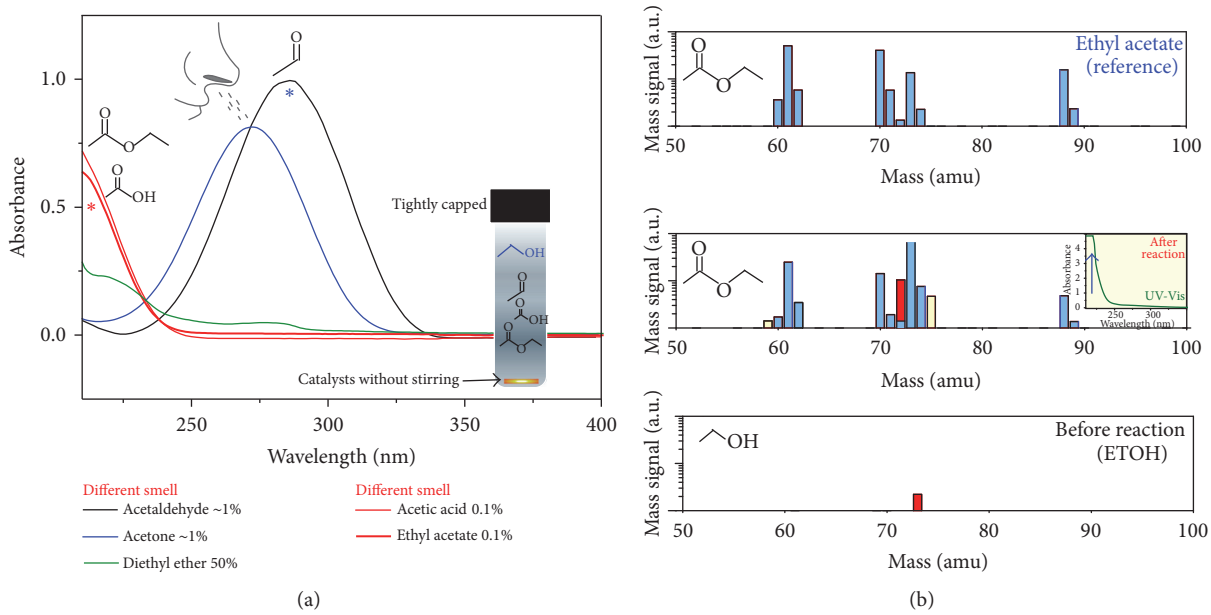

Figure 8: UV-Vis absorption spectra (a) of standard samples of acetaldehyde (1%), acetone (1%), acetic acid (0.1%), and ethyl acetate (0.1%). Mass spectra (b) of reference samples (ethyl acetate and ethanol) and the solution sample after reaction. The inset shows the UV-Vis absorption spectrum of the corresponding sample solution. Blue and red ∗ indicate the peak positions for acetaldehyde and ethyl acetate, respectively.

was that the catalytic efficiency of doped and codoped CeO_2 was tested for both gas-phase CO and liquid-phase ethanol oxidation reactions. For the 1st and 2nd runs of bare CeO_2, $T_{10\%}$ was observed at 405°C. $T_{10\%}$ of bare CeO_2 for CO oxidation was lowered significantly by 165°C upon metal (Ag/Au = 1/4 mol.%) doping. There were some synergic effects upon codoping for the CO oxidation. The CO oxidation activity varies with the relative concentrations of two different metals. Sintering and alloying of two different metals were found to play important roles in the CO oxidation activity.

For liquid-phase ethanol oxidation, two liquid products of ethyl acetate (major, λ_{max} = 220 nm) and acetaldehyde (minor, λ_{max} = 280 nm) were observed by UV-Vis absorption spectroscopy. The concentration of acetaldehyde (CH_3CHO) reached a saturation point, while that of ethyl acetate ($CH_3COOCH_2CH_3$) dramatically increased with reaction time. These findings indicate that acetaldehyde species promptly undergo further reaction to form a major product, ethyl acetate, which was confirmed by mass spectrometry and UV-visible absorption. Undoped CeO_2 produces negligible acetaldehyde, which is direct evidence that a hydride shift reaction, $CH_3CH_2O(ad)\text{-}M \rightarrow CH_2CHO + MH$, is an important step for acetaldehyde production for metal-loaded CeO_2 catalysts. For M- (single) doped CeO_2 NPs, the ethanol oxidation performance showed an order of Ni < Ag < Pd ≪ Au. For MM′ codoped CeO_2 NPs, the activity of Au doped CeO_2 deteriorated drastically upon adding another metals (Ag, Ni, and Pd) as cocatalyst. The Au-rich CeO_2 catalyst showed higher catalytic activity. On the other hand, the Ni/Pd codoped sample showed much higher catalytic activity, compared with the single M- (Ni and Pd) doped samples. This study provides further insights into the development of catalysts applicable to a range of oxidation reactions.

Competing Interests

The authors declare no conflict of interests.

Acknowledgments

This study was supported by the 2015 Yeungnam University Research Grant.

References

[1] X. Nie, H. Qian, Q. Ge, H. Xu, and R. Jin, "CO oxidation catalyzed by oxide-supported $Au_{25}(SR)_{18}$ nanoclusters and

identification of perimeter sites as active centers," *ACS Nano*, vol. 6, no. 7, pp. 6014–6022, 2012.

[2] H.-F. Li, N. Zhang, P. Chen, M.-F. Luo, and J.-Q. Lu, "High surface area Au/CeO_2 catalysts for low temperature formaldehyde oxidation," *Applied Catalysis B: Environmental*, vol. 110, pp. 279–285, 2011.

[3] K. Y. Ho and K. L. Yeung, "Effects of ozone pretreatment on the performance of Au/TiO_2 catalyst for CO oxidation reaction," *Journal of Catalysis*, vol. 242, no. 1, pp. 131–141, 2006.

[4] K. Y. Ho and K. L. Yeung, "Properties of TiO_2 support and the performance of Au/TiO_2 catalyst for CO oxidation reaction," *Gold Bulletin*, vol. 40, no. 1, pp. 15–30, 2007.

[5] J. Qi, J. Chen, G. Li, S. Li, Y. Gao, and Z. Tang, "Facile synthesis of core-shell $Au@CeO_2$ nanocomposites with remarkably enhanced catalytic activity for CO oxidation," *Energy and Environmental Science*, vol. 5, no. 10, pp. 8937–8941, 2012.

[6] D. Jiang, W. Wang, L. Zhang, Y. Zheng, and Z. Wang, "Insights into the surface-defect dependence of photoreactivity over CeO_2 nanocrystals with well-defined crystal facets," *ACS Catalysis*, vol. 5, no. 8, pp. 4851–4858, 2015.

[7] W. Lei, T. Zhang, L. Gu et al., "Surface-structure sensitivity of CeO_2 nanocrystals in photocatalysis and enhancing the reactivity with nanogold," *ACS Catalysis*, vol. 5, no. 7, pp. 4385–4393, 2015.

[8] B. Li, T. Gu, T. Ming, J. Wang, P. Wang, and J. C. Yu, "Gold core)@(ceria shell) nanostructures for plasmon-enhanced catalytic reactions under visible light," *ACS Nano*, vol. 8, no. 8, pp. 8152–8162, 2014.

[9] P. Lu, B. Qiao, N. Lu et al., "Photochemical deposition of highly dispersed Pt nanoparticles on porous CeO_2 nanofibers for the water-gas shift reaction," *Advanced Functional Materials*, vol. 25, no. 26, pp. 4153–4162, 2015.

[10] L. Meng, A.-P. Jia, J.-Q. Lu, L.-F. Luo, W.-X. Huang, and M.-F. Luo, "Synergetic effects of PdO species on CO oxidation over $PdO-CeO_2$ catalysts," *Journal of Physical Chemistry C*, vol. 115, no. 40, pp. 19789–19796, 2011.

[11] Y. Park, S. K. Kim, D. Pradhan, and Y. Sohn, "Thermal H_2-treatment effects on CO/CO_2 conversion over Pd-doped CeO_2 comparison with Au and Ag-doped CeO_2," *Reaction Kinetics, Mechanisms and Catalysis*, vol. 113, no. 1, pp. 85–100, 2014.

[12] Y. Park, S. K. Kim, D. Pradhan, and Y. Sohn, "Surface treatment effects on CO oxidation reactions over Co, Cu, and Ni-doped and codoped CeO_2 catalysts," *Chemical Engineering Journal*, vol. 250, pp. 25–34, 2014.

[13] B. Xu, Q. Zhang, S. Yuan, M. Zhang, and T. Ohno, "Morphology control and photocatalytic characterization of yttrium-doped hedgehog-like CeO_2," *Applied Catalysis B: Environmental*, vol. 164, pp. 120–127, 2015.

[14] W. Huang and Y. Gao, "Morphology-dependent surface chemistry and catalysis of CeO_2 nanocrystals," *Catalysis Science and Technology*, vol. 4, no. 11, pp. 3772–3784, 2014.

[15] Y. Gao, W. Wang, S. Chang, and W. Huang, "Morphology effect of CeO_2 support in the preparation, metal-support interaction, and catalytic performance of Pt/CeO_2 catalysts," *ChemCatChem*, vol. 5, no. 12, pp. 3610–3620, 2013.

[16] Y. Zhang, N. Zhang, Z.-R. Tang, and Y.-J. Xu, "A unique silk mat-like structured Pd/CeO_2 as an efficient visible light photocatalyst for green organic transformation in water," *ACS Sustainable Chemistry & Engineering*, vol. 1, no. 10, pp. 1258–1266, 2013.

[17] W. G. Shin, H. J. Jung, H. G. Sung, H. S. Hyun, and Y. Sohn, "Synergic CO oxidation activities of boron-CeO_2 hybrid materials prepared by dry and wet milling methods," *Ceramics International*, vol. 40, no. 8, pp. 11511–11517, 2014.

[18] H. Wu, P. Wang, H. He, and Y. Jin, "Controlled synthesis of porous Ag/Au bimetallic hollow nanoshells with tunable plasmonic and catalytic properties," *Nano Research*, vol. 5, no. 2, pp. 135–144, 2012.

[19] N. Sasirekha, P. Sangeetha, and Y.-W. Chen, "Bimetallic Au–Ag/CeO_2 catalysts for preferential oxidation of CO in hydrogen-rich stream: effect of calcination temperature," *The Journal of Physical Chemistry C*, vol. 118, no. 28, pp. 15226–15233, 2014.

[20] S. Chen, L. Luo, Z. Jiang, and W. Huang, "Size-dependent reaction pathways of low-temperature CO oxidation on Au/CeO_2 catalysts," *ACS Catalysis*, vol. 5, no. 3, pp. 1653–1662, 2015.

[21] D. Liu, W. Li, X. Feng, and Y. Zhang, "Galvanic replacement synthesis of $Ag_xAu_{1-x}@CeO_2(0 \leq x \leq 1)$ core@shell nanospheres with greatly enhanced catalytic performance," *Chemical Science*, vol. 6, pp. 7015–7019, 2015.

[22] Y. Kang, M. Sun, and A. Li, "Studies of the catalytic oxidation of CO over Ag/CeO_2 catalyst," *Catalysis Letters*, vol. 142, no. 12, pp. 1498–1504, 2012.

[23] S. Chang, M. Li, Q. Hua et al., "Shape-dependent interplay between oxygen vacancies and Ag–CeO_2 interaction in Ag/CeO_2 catalysts and their influence on the catalytic activity," *Journal of Catalysis*, vol. 293, pp. 195–204, 2012.

[24] R. Fiorenza, C. Crisafulli, G. G. Condorelli, F. Lupo, and S. Scirè, "Au-Ag/CeO_2 and Au-Cu/CeO_2 Catalysts for volatile organic compounds oxidation and CO preferential oxidation," *Catalysis Letters*, vol. 145, no. 9, pp. 1691–1702, 2015.

[25] J. Zhang, L. Li, X. Huang, and G. Li, "Fabrication of Ag–CeO_2 core-shell nanospheres with enhanced catalytic performance due to strengthening of the interfacial interactions," *Journal of Materials Chemistry*, vol. 22, no. 21, pp. 10480–10487, 2012.

[26] A. Leyva-Pérez, D. Cómbita-Merchán, J. R. Cabrero-Antonino, S. I. Al-Resayes, and A. Corma, "Oxyhalogenation of activated arenes with nanocrystalline ceria," *ACS Catalysis*, vol. 3, no. 2, pp. 250–258, 2013.

[27] Y. Liu, H. Li, J. Yu, D. Mao, and G. Lu, "Electronic storage capacity of ceria: role of peroxide in Aux supported on $CeO_2(111)$ facet and CO adsorption," *Physical Chemistry Chemical Physics*, vol. 17, no. 41, pp. 27758–27768, 2015.

[28] D. Jiang, W. Wang, S. Sun, L. Zhang, and Y. Zheng, "Equilibrating the plasmonic and catalytic roles of metallic nanostructures in photocatalytic oxidation over Au-modified CeO_2," *ACS Catalysis*, vol. 5, no. 2, pp. 613–621, 2015.

[29] M. M. Khan, S. A. Ansari, M. O. Ansari, B. K. Min, J. Lee, and M. H. Cho, "Biogenic fabrication of $Au@CeO_2$ nanocomposite with enhanced visible light activity," *Journal of Physical Chemistry C*, vol. 118, no. 18, pp. 9477–9484, 2014.

[30] A. Tanaka, K. Hashimoto, and H. Kominami, "Preparation of Au/CeO_2 exhibiting strong surface plasmon resonance effective for selective or chemoselective oxidation of alcohols to aldehydes or ketones in aqueous suspensions under irradiation by green light," *Journal of the American Chemical Society*, vol. 134, no. 35, pp. 14526–14533, 2012.

[31] H. Y. Kim, H. M. Lee, and G. Henkelman, "CO oxidation mechanism on CeO_2-supported Au nanoparticles," *Journal of the American Chemical Society*, vol. 134, no. 3, pp. 1560–1570, 2012.

[32] A. Maldotti, A. Molinari, R. Juárez, and H. Garcia, "Photoinduced reactivity of Au–H intermediates in alcohol oxidation by

gold nanoparticles supported on ceria," *Chemical Science*, vol. 2, no. 9, pp. 1831–1834, 2011.

[33] L. Vivier and D. Duprez, "Ceria-based solid catalysts for organic chemistry," *ChemSusChem*, vol. 3, no. 6, pp. 654–678, 2010.

[34] N. Zhang, S. Liu, X. Fu, and Y.-J. Xu, "A simple strategy for fabrication of "plum-pudding" type Pd@CeO_2 semiconductor nanocomposite as a visible-light-driven photocatalyst for selective oxidation," *Journal of Physical Chemistry C*, vol. 115, no. 46, pp. 22901–22909, 2011.

[35] Y. Sohn, "SiO_2 nanospheres modified by Ag nanoparticles: surface charging and CO oxidation activity," *Journal of Molecular Catalysis A: Chemical*, vol. 379, pp. 59–67, 2013.

[36] W. J. Kim, D. Pradhan, and Y. Sohn, "Fundamental nature and CO oxidation activities of indium oxide nanostructures: 1D-wires, 2D-plates, and 3D-cubes and donuts," *Journal of Materials Chemistry A*, vol. 1, no. 35, pp. 10193–10202, 2013.

[37] R.-R. Zhang, L.-H. Ren, A.-H. Lu, and W.-C. Li, "Influence of pretreatment atmospheres on the activity of Au/CeO_2 catalyst for low-temperature CO oxidation," *Catalysis Communications*, vol. 13, no. 1, pp. 18–21, 2011.

[38] Y. Li, Y. Cai, X. Xing, N. Chen, D. Deng, and Y. Wang, "Catalytic activity for CO oxidation of Cu–CeO_2 composite nanoparticles synthesized by a hydrothermal method," *Analytical Methods*, vol. 7, no. 7, pp. 3238–3245, 2015.

[39] R. Shang, Y. Duan, X. Zhong, W. Xie, Y. Luo, and L. Huang, "Formic acid modified Co_3O_4-CeO_2 catalysts for CO oxidation," *Catalysts*, vol. 6, no. 3, p. 48, 2016.

[40] A. Abad, P. Concepción, A. Corma, and H. García, "A collaborative effect between gold and a support induces the selective oxidation of alcohols," *Angewandte Chemie—International Edition*, vol. 44, no. 26, pp. 4066–4069, 2005.